An Operational Concept for Correcting Navigation Drift during Sonar Surveys of the Seafloor

Alan J. Hunter, *Member, IEEE*, Warren A. Connors and Samantha Dugelay

***Abstract*—The accumulation of navigation errors (drift) is a problem in many applications of autonomous underwater vehicles, particularly during long-duration underwater surveys. Traditional methods for correcting drift require either surfacing of the vehicle for a GNSS update or use of an independent acoustic positioning system. These methods may not be desirable or possible due to mission constraints. We propose a solution to this problem completely underwater and without the aid of external navigation systems. The approach is based on an operational concept that uses a modified paired-track survey pattern combined with through-the-sensor navigation corrections from a seafloor imaging sonar. We describe the operational concept, derive a model for its performance limits, validate this model, and demonstrate the concept with real experiments at sea. Using this approach, we provide an opportunity to use either coherent or incoherent through-the-sensor positioning corrections for a mission length increase of only the product of the intra-track spacing and the number of track pairs. We show results from a proof-of-principle experiment using data collected by the 300 kHz synthetic aperture sonar of the NATO Centre for Maritime Research and Experimentation's MUSCLE AUV.**

***Index Terms*—Autonomous underwater vehicle, underwater navigation, drift correction, SLAM, synthetic aperture sonar, micronavigation**

I. Introduction

APPLICATIONS of autonomous underwater vehicles (AUVs) often require very accurate measurements of vehicle location and pose. A good example is when localising and, subsequently, relocalising objects on the seafloor. Errors in the AUV's assumed location and pose during object localisation translate into errors in the perceived positions of the objects. These errors can lead to difficulties when subsequently relocalising the objects, possibly requiring an extended search period or preventing relocalisation altogether. Examples of areas where accurate underwater search and localisation are important include oil and gas field monitoring, search and recovery, underwater archeology, and naval mine counter-measures. With the increase in capability and reliability of robotic platforms, their applicability to these fields has been increasing at a considerable rate.

Consider naval mine counter-measures (MCM) as an illustrative use case. The use of multiple heterogeneous AUVs in MCM means that one platform may be assigned to the initial search, i.e., detection and classification of bottom objects, and another independent platform used for reacquisition and identification of the targets. This results in a need for accurate navigation and localisation, particularly in challenging seafloor environments where many clutter objects may exist. Furthermore, as in the other applications mentioned above, an MCM mission requires the planning of a survey pattern which will achieve or exceed a minimum probability of detecting the intended targets. In cases where the variance on the navigation error is unbounded, this planning may not be possible, or only achievable with a considerable amount of overlap in the sensor footprint, thus reducing efficiency.

The underwater environment creates a challenge for navigation due to the inaccessibility of global navigation satellite systems (GNSS). In the underwater domain, positioning has typically been provided by dead-reckoning from on-board sensor measurements or by use of external systems for acoustic positioning.

In dead-reckoning, an AUV estimates its position relative to a known starting position from measurements of pose and integrated measurements of velocity [1]. Commonly, the pose is measured using accelerometers, gyroscopes, and magnetic sensors, and the velocities are measured using a Doppler Velocity Log (DVL). An optimal fusion of these measurements can be made using a kinematic state estimation algorithm, e.g., a Kalman filter, and this combined system is referred to as a DVL-aided inertial navigation system (INS) [2]. Navigation solutions based on dead-reckoning, such as DVL-aided INS, contain sources of measurement error which accumulate over time – this is known as navigation "drift". To bound these errors in underwater surveys where a high level of accuracy is required, it is common to employ the operational strategy of surfacing regularly (e.g., at the beginning of each track) for a navigation update from a GNSS.

External systems for acoustic positioning include long, short, and ultra-short baseline (LBL, SBL, and USBL) systems [3]. These systems use a network of assets with acoustic transponders at known positions, typically in the form of vessels or buoys on the sea surface equipped with GNSS sensors or fixed nodes on the bottom. Positioning measurements are made and communicated to the AUV through the transmission and reception of acoustic signals. An advantage of this approach is that measurement errors do not accumulate over time. However, the requirement for fielding additional assets constrains its utility. In large or potentially dangerous search areas, it may not be feasible to deploy the system or, for missions over a large area, a prohibitively large number of assets may be required to provide sufficient coverage.

Recent innovations in underwater navigation have been based on so-called "data-driven" or "through-the-sensor" ap-

A. Hunter is with the of University of Bath, Claverton Down Rd, Bath, Somerset BA2 7AY, United Kingdom; e-mail: a.j.hunter@bath.ac.uk.

W. Connors and S. Dugelay are with the NATO Science and Technology Organization, Centre for Maritime Research and Experimentation, Viale San Bartolomeo 400, 19126 La Spezia, Italy.

proaches. These exploit data collected by the payload sensor which, in the underwater domain, is commonly a sonar system. An early example is terrain navigation, where sonar bathymetry measurements are matched with a bathymetric map stored on the vehicle and differences between the observed and mapped bathymetry are used to update the navigation solution. This approach has been demonstrated using multibeam sonar [4], [5]. However, a limitation is that a sufficiently accurate and precise map of the search area is required *a priori*. More recently, simultaneous localisation and mapping (SLAM) [6] methods have extended the approach, enabling mobile robots to select robust features dynamically from the data and use these to navigate. An early example for side-scan sonar used manual operator-generated landmarks [7]. SLAM has since been demonstrated autonomously with sector-scan sonar [8], [9], [10], [11], [12], multibeam sonar [13], [14], [15], [16], and side-scan sonar [17], [18].

Micro-navigation is a related data-driven approach which exploits redundant phase information in the coherent echo data collected at overlapping portions of the sonar array between subsequent pings [19]. It can provide relative navigation corrections with sub-wavelength precision (i.e., on order of millimeters to hundreds of micrometers at typical operating frequencies of hundreds of kilohertz) and has been a key enabler for synthetic aperture sonar (SAS) processing [20]. It has also been used to enhance DVL-aided INS navigation [21].

Recent work in micro-navigation has achieved sub-wavelength precision over repeated passes [22], [23]. This can be considered a coherent extension of the SLAM method offering higher precision. Moreover, an advantage of operating on coherent data (as opposed to incoherent bathymetry maps or images used in conventional SLAM) is that the ubiquitous speckle patterns scattered by the seafloor are used without reliance on geometric seafloor features, which may not be present or reliable in benign environments. A disadvantage, however, is that speckle patterns are sensitive to angular decorrelation of the scattered field [24] and temporal decorrelation of the seafloor [25].

Data-driven navigation shows considerable promise, particularly for deep or covert operations, since it permits the correction of drift without the need to surface for a GNSS fix. However, regardless of whether incoherent or coherent methods are used, the vehicle must revisit specific areas of seafloor in order to perform these corrections. Each revisit requires the expenditure of valuable mission resources (i.e., energy and time) with no new information added to the overall search task. Therefore, to provide an effective solution, the mission plan must be selected carefully to achieve the revisits required to maintain the desired level of navigation accuracy but without adding a considerable increase on the overall distance traveled or mission duration. To this end, we introduce a new operational concept that leverages data-driven navigation methods together with a novel modification to a paired-track survey pattern.

The operational concept is introduced in Section II, covering the proposed modifications to the paired-track survey pattern and methods of data-driven navigation correction. In Section III, we describe a simple Monte-Carlo approach for modeling the accumulation of navigation errors within both conventional underwater surveys and surveys that employ the new concept. Experimental data are presented in Section IV and used as a proof-of-principle as well as validating and tuning the Monte-Carlo model. In Section V, projections of the expected performance improvements offered by the new concept are explored using the model. Finally, we discuss the results and their potential operational impact in Section VI and offer conclusions in Section VII.

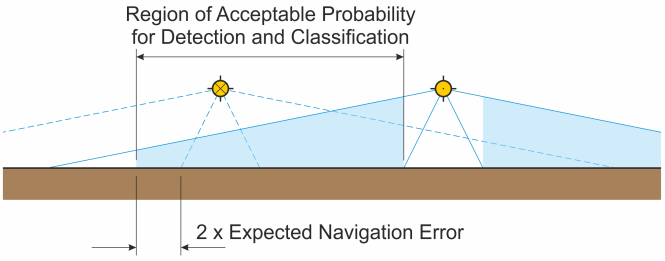

Fig. 1: A paired-track side-scan survey pattern ensures that the swaths of track pairs cover the nadir gaps of one another.

II. Operational Concept

An effective underwater search requires a consistent coverage of the seafloor that achieves or exceeds a required minimum probability of detecting any target objects. This probability of detection is influenced not only by sensor performance parameters, such as signal-to-noise ratio and resolution, but also the mission plan which aims to ensure there are no gaps in sensor coverage over the search area. Coverage gaps can be caused by limitations in the footprint of the sensor as well as limitations in the navigational accuracy of the vehicle. Effective mission planning must take into account both of these sensor and vehicle characteristics to ensure the required coverage.

Using the example of an MCM mission, search patterns have been defined which take into account the footprint of the sensor, but also the expected variance on the navigation error for the sensor platform, known as the standard deviation on navigation error (SDNE). For surface vessels equipped with GNSS, this navigation variance can be relatively static. This allows for the development of a track plan which contains sufficient overlap to ensure consistent coverage for satisfying the probability of detection of underwater objects. For underwater platforms such as AUVs, for which GNSS is not available, the variance on navigation error is dynamic, varying with many factors, including the mission length and type. This requires special consideration for the track placements to ensure no gaps in the sensor coverage. Furthermore, most AUVs are equipped with side looking sonars, where an area directly under the sonar, the nadir, exists in which the sensor performance is too low for detection or classification of objects of interest. To cover this gap requires either a gap-filling sensor (e.g., a multibeam sonar) or a specific mission plan. Consideration of the navigation error is key for both effective sensor coverage and for the utility of the position estimates

resulting from the search. In this work, it is assumed that a gap filling sensor is not used, and therefore techniques for mission planning which ensure coverage of the nadir must be employed.

A. Paired-Track Pattern

Paired-track mission planning is an approach for ensuring gap-free seafloor coverage using a side-looking sonar. It is based on a combination of two tracks that are offset such that the sensor footprint from one is effectively covering the nadir of the other. Figure 1 illustrates the concept. The resulting search pattern is comprised of a series of track pairs and provides full coverage of the search area. Figure 2a illustrates a paired-track pattern.

A limitation of the approach is that it depends on a static approximation for the expected navigation error to avoid either excessive overlap in the sensor coverage or gaps. As the navigation error variance is dynamic during mission execution due to drift, there is a risk of underestimating the navigation error and potentially causing gaps in the sensor coverage.

B. Modified Paired-Track Pattern

In order to employ data-driven navigation correction during a search mission, there must be opportunities within the search pattern to revisit regions of the seafloor from the same aspect. Ideally, these revisits should be brief to minimise redundant data collection but long enough to ensure the correct determination of navigation error. They should also occur often and regularly to limit the drift rate. We propose a simple modification to the paired-track pattern that satisfies these requirements.

Our modified paired-track pattern uses a simple reordering of waypoints, as illustrated in Figure 2b. This introduces overlaps during the transit paths at the end of each track pair (e.g., along the path between waypoints 1-2 and the first portion of the path between waypoints 5-6 in Figure 2b). These overlapping paths presents regular opportunities for data-driven navigation correction throughout the execution of the pattern. The cost is an increase in the mission duration commensurate with twice the intra-pair spacing for every track pair. However, in a typical survey, the track lengths are considerably longer than the intra-pair spacing and this increase will be minimal.

The data-driven methods require adequate sensor overlap during repeated passes to enable robust estimation of the navigation errors and their subsequent correction. It is possible that this condition might not be satisfied when the tracks are too long. The navigation drift between revisits could be so large that the same area of seafloor is not observed or that it is viewed from a significantly different angle. This will impact the various methods in different ways. In any case, we propose a further modification to the paired-track pattern to address this potential problem.

An alternative split variation of the modified paired-track pattern is shown in Figure 2c. This approach splits surveys with long tracks into two modified paired-track patterns with half the track length. Thus, it halves the time between revisits

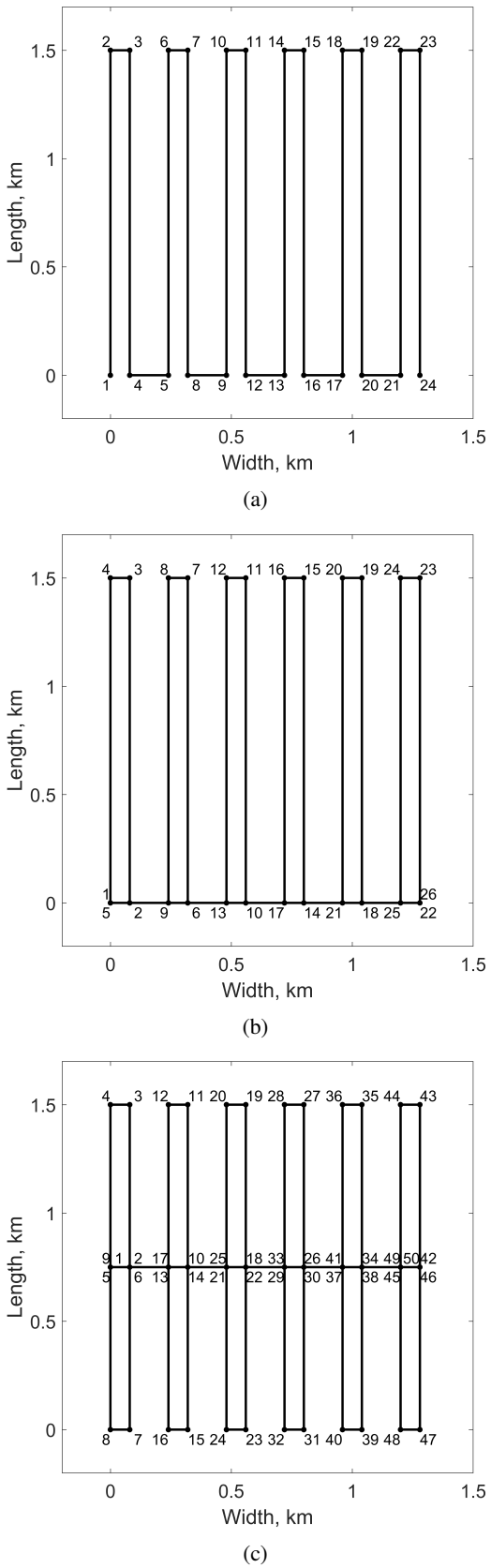

Fig. 2: A conventional paired-track pattern is shown in (a) with numbers denoting the waypoint indices. Our proposed modifications to the pattern are shown in (b) and (c) with minimal overlap at the ends of the tracks allowing repeat-pass drift correction to be applied after executing each track pair.

and, consequently, reduces the drift rate. However, there are tradeoffs. It further lengthens the mission duration by four times (instead of twice) the intra-pair spacing for each track pair. Moreover, it introduces a small coverage gap centrally along the width of the survey area. This gap may necessitate a final track along the width of the pattern to ensure complete coverage. The pattern splitting principle can be further generalised to deal with survey patterns of arbitrary length. An ideal track length can be determined and used to define a sub-pattern. This sub-pattern can then be repeated as necessary to achieve the desired overall length.

C. Data-Driven Navigation Correction Methods

There are opportunities for data-driven navigation correction at each of the redundant overlapping portions in the modified paired-track patterns proposed in Section II-B or other patterns based on the same general idea. During these repeated passes, a variery of algorithms can be used to estimate the accumulation of navigation errors relative to the previous pass. We consider two different approaches here. One is based on cross-correlation of the incoherent sonar imagery and the other is based on repeat-pass micronavigation using coherent SAS data. Other possible methods include, but are not limited to landmark recognition [17], [18] or image feature-matching [26], [27].

1) Image Correlation (Incoherent): A simple approach is to perform a 2-D cross-correlation between intensity images acquired from each of the repeated passes. The relative accumulation of navigation errors in the along-track and across-track directions can then be estimated by locating the peak in the correlation function, i.e.,

$$\tilde{\mathbf{x}} - \mathbf{x} \;\approx\; \arg\max_{\boldsymbol{\zeta}} \left\{ \iint_{-\infty}^{\infty} I_1(\mathbf{u})\, I_2(\mathbf{u}+\boldsymbol{\zeta})\; \mathrm{d}\mathbf{u} \right\}, \quad (1)$$

where $I_1(\mathbf{u})$ and $I_2(\mathbf{u})$ are the registered images from the repeated passes. Before cross-correlating, the images must be registered to a common coordinate frame using the measurements available from the navigation hardware. In this way, compensation is made for the known differences in acquisition geometry and, thus, permitting the residual differences observed in the correlation function to be attributed to the relative navigation errors. The registration must correct for bulk translation and rotation of the images caused by path offsets in along-track, across-track, and heading. It must also correct for image distortions caused by variations in motions such as surge, sway, and yaw along the paths (e.g., skewing caused by vehicle "crabbing" in currents). Furthermore, if SAS focusing is employed then the corrections introduced by intra-pass micronavigation must also be accommodated.

There are some limitations to this approach. It relies on sufficient seafloor texture (e.g., sand ripples, debris, vegetation boundaries, etc.) to generate an adequate peak in the correlation function. Therefore, it can fail on benign seafloor environments. Also, the performance will degrade when the differences in acquisition geometry are large enough that they result in significant changes in the image projections (e.g., causing the lengthening / shortening of shadows cast from the seafloor bathymetry and proud objects) and variations in acoustic scattering properties. Similar limitations are inherent to methods based on feature matching and landmark recognition.

2) Repeat-Pass RPC Micronavigation (Coherent): Redundant phase center (RPC) or displaced phase center antenna (DPCA) micronavigation [19] has been a crucial enabler for SAS imaging. It is a data-driven estimation of the relative motion between subsequent pings, utilizing the coherent sonar echo data measured by the physical sonar array. Very high, sub-wavelength precision can be achieved using this approach. Recent work has extended the technique to measure the relative geometry for pings between repeated passes [22], [23]. In addition to permitting sub-wavelength co-registration of SAS data for repeat-pass interferometry, this provides a means of estimating precisely the relative navigation errors accumulated between the repeated passes.

The precision of this coherent approach is orders of magnitude better than the incoherent image correlation approach of Section II-C1. However, it is less robust to differences in the data acquisition geometries between the passes. In particular, inter-pass sway and yaw can reduce coherence and cause the method to fail [24].

	Standard Deviation		Time Constant	
DVL Velocity				
Measurement Noise	$\sigma_{v,\mathrm{noise}}$	$5\ \mathrm{mm/s}$	-	-
Bias Error	$\sigma_{v,\mathrm{bias}}$	$1\ \mathrm{mm/s}$	$\tau_{v,\mathrm{bias}}$	$30\ \mathrm{min}$
Scale Factor	σ_S	$0.2\ \%$	τ_S	$30\ \mathrm{min}$
Gyro Heading				
Bias Error	σ_θ	$\frac{0.02}{\cos\phi}\ \mathrm{deg}$	τ_θ	$60\ \mathrm{min}$

TABLE I: Parameters used for the navigation error modelling. Standard deviation values for the DVL are taken from the Teledyne RDI-600 Workhorse Navigator datasheet [29]; a typical standard deviation for the gyro-compass heading (where the variable ϕ is the latitude in radians) and typical time constants are taken from [2].

III. Navigation Error Modeling

The benefits of using different operational concepts can be explored by use of a navigation error model. A model is presented here and the resulting performance prediction is given in Section V over a range of relevant scenarios.

Sophisticated commercial software exists for modeling the navigation errors in various navigation solutions (e.g., NavLab [28]). However, to gain insight into the problem, we have chosen to use a simple Monte-Carlo simulation, which is described in Section III-A and validated with experimental data in Section IV-B. Many commercial AUVs use DVL-aided INS to navigate underwater and we assume this common navigation solution in the following analysis. Other solutions are not considered but can, in principle, be approached using the same methodology.

A. Monte-Carlo Simulations

The positioning errors from a DVL-aided INS are dominated by integrated ground-velocity errors from the DVL and

heading errors from the gyro-compass. Typically, product manufacturers model these errors as Gaussian-distributed random variables [2], [30]. The ground-velocity errors are comprised of a white measurement noise with zero mean and variance $\sigma^2_{v,\mathrm{noise}}$, and coloured noise for the scale factor and bias errors with zero mean, variances σ^2_S and $\sigma^2_{v,\mathrm{bias}}$, and time constants τ_S and $\tau_{v,\mathrm{bias}}$, respectively. Similarly, the bias error for the heading is modelled as coloured noise with variance σ^2_θ and time constant τ_θ. Some published statistics for a high-end DVL-aided INS are given in Table I.

The AUV position is estimated by accumulating the ground-velocity measurements. The $n\mathrm{th}$ position estimate at time $t\,[n] = n\Delta t$ is given by

$$\tilde{\mathbf{x}}\,[n] = \mathbf{x}\,[0] + \sum_{m=1}^{n} \mathbf{R}\,[m]\,\tilde{\mathbf{v}}\,[m]\,\Delta t \tag{2}$$

where $\mathbf{x}\,[0]$ is the initial position measurement (e.g., made at the sea surface via GNSS),

$$\tilde{\mathbf{v}}\,[m] = (1 + S\,[m])\,\mathbf{v}\,[m] + \mathbf{v}_{\mathrm{bias}}\,[m] + \mathbf{v}_{\mathrm{noise}}\,[m] \tag{3}$$

is the $m\mathrm{th}$ ground-velocity measurement with respect to the AUV fixed-body and $\mathbf{v}\,[m]$ is the true ground-velocity. The matrix

$$\mathbf{R}\,[m] = \begin{pmatrix} \cos\,\tilde{\theta}\,[m] & -\sin\,\tilde{\theta}\,[m] \\ \sin\,\tilde{\theta}\,[m] & \cos\,\tilde{\theta}\,[m] \end{pmatrix} \tag{4}$$

describes the measured rotation from the fixed-body to inertial coordinate frame, where

$$\tilde{\theta}\,[m] = \theta\,[m] + \theta_{\mathrm{bias}}\,[m] \tag{5}$$

is the measured heading, $\theta\,[m]$ is the true heading, and the rotations in pitch and roll are ignored.

The ground-velocity measurement noise $\mathbf{v}_{\mathrm{noise}} = (v_{\mathrm{noise},x}, v_{\mathrm{noise},y})$ has independent Gaussian-distributed components that are uncorrelated in time, i.e.,

$$v_{\mathrm{noise},x}\,[m]\,, v_{\mathrm{noise},y}\,[m] \sim \mathcal{N}\,\{0, \sigma_{v,\mathrm{noise}}\}\,, \tag{6}$$

where $\mathcal{N}\,\{\mu, \sigma\}$ denotes a Gaussian distribution with mean μ and variance σ^2. The ground-velocity scale factor S, bias error $\mathbf{v}_{\mathrm{bias}} = (v_{\mathrm{bias},x}, v_{\mathrm{bias},y})$, and heading bias error θ_{bias} are independent Markov processes, i.e.,

$$S\,[m] \sim \mathcal{M}\,\{0, \sigma_S, \tau_S; S\,[m-1]\} \tag{7}$$

$$v_{\mathrm{bias},x}\,[m] \sim \mathcal{M}\,\{0, \sigma_{v,\mathrm{noise}}, \tau_{v,\mathrm{bias}}; v_{\mathrm{bias},x}\,[m-1]\} \tag{8}$$

$$v_{\mathrm{bias},y}\,[m] \sim \mathcal{M}\,\{0, \sigma_{v,\mathrm{noise}}, \tau_{v,\mathrm{bias}}; v_{\mathrm{bias},y}\,[m-1]\} \tag{9}$$

$$\theta_{\mathrm{bias}}\,[m] \sim \mathcal{M}\,\{0, \sigma_\theta, \tau_\theta; \theta_{\mathrm{bias}}\,[m-1]\}\,, \tag{10}$$

where $\mathcal{M}\,\{\mu, \sigma, \tau, U_{m-1}\}$ denotes a Markov sequence with time constant τ and time step Δt. The $m\mathrm{th}$ value U_m in the sequence is generated by the iteration

$$U_m = \rho\,U_{m-1} + \left[\sigma\sqrt{1-\rho^2}\right] W_m, \tag{11}$$

where

$$\rho = \exp\left(-\frac{\Delta t}{\tau}\right), \tag{12}$$

is the correlation kernel, and

$$W_m, U_0 \sim \mathcal{N}\,\{\mu, \sigma\}\,, \tag{13}$$

are uncorrelated Gaussian-distributed random variables [31].

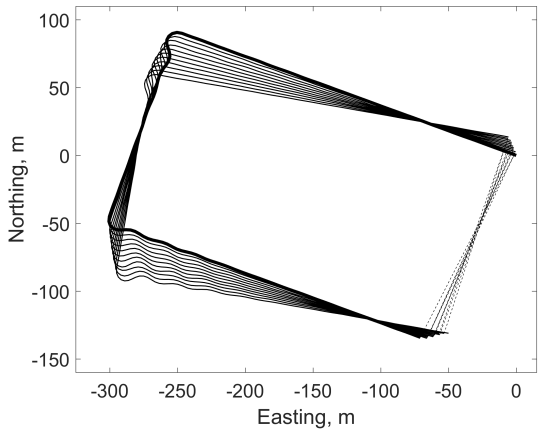

Fig. 3: A two-track pattern, repeated eleven times in $1\,\mathrm{deg}$ heading increments (22 tracks total). The tracks have lengths of $330\ \mathrm{m}$ and are separated by $150\ \mathrm{m}$. The first pattern is indicated by the thick line.

B. Navigation Correction

In the proposed concept, navigation corrections are performed at every opportunity where redundant data is collected from a repeated pass. During these passes, a data-driven method is used to estimate and correct the measurable drift that has accumulated since the previous pass. In practice, the estimation procedure will either succeed or fail and, in cases where it succeeds, some measurement errors will be introduced. The success or failure of the correction and the properties of the measurement errors will depend on the choice of estimation method and a variety of geometric and environmental factors. Quantifying this is beyond the scope of this work. For this reason, we have adopted a simplified model.

When an estimate is made successfully, it is reasonable to assume that the associated measurement errors will be smaller than the accumulated drift and can be neglected, resulting in an ideal update to the navigation solution. In the case of a successful estimate, the current position is updated using the position estimated in the previous pass, which was less affected by accumulated drift. Otherwise, it is left unchanged. Each successful update also offers the opportunity to retroactively correct the preceding position estimates. Here, we simply perform the dead-reckoning in reverse from the updated position by accumulating the velocity estimates (2) backwards in time. In practice, this would be better achieved by operating a Kalman Filter in reverse (e.g., [7]) and possibly also estimating and compensating the correlated errors.

The success or failure of each update is modelled by evaluating a sample drawn from a uniform random distribution against a probability, which is defined as a function of the relevant influencing factors. A key factor affecting the success of the estimation is the across-track displacement between passes. Despite the planned pattern, this inter-pass sway will be non-zero due to possible platform instabilities and navigation drift accumulated during the transit of the tracks between updates. We have prescribed a simple model for the probability of success with respect to inter-pass sway y. This follows a

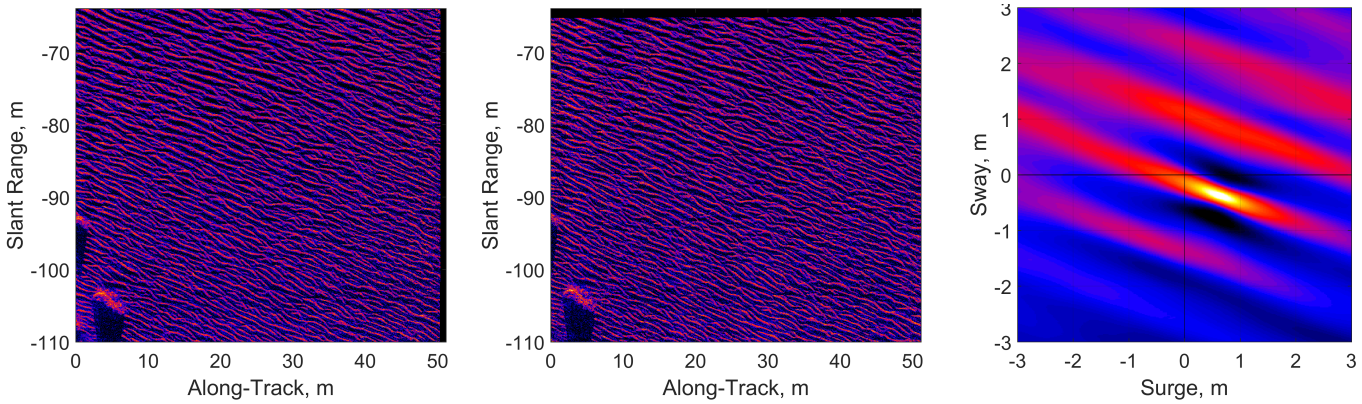

(a) (b) (c)

Fig. 4: SAS image correlation for sub-images from (a) the 11th track and (b) the 13th track, adjusted for the corrections introduced by (intra-pass) RPC micronavigation and projected to a common coordinate frame using measurements from the navigation hardware; (c) 2-D cross-correlation, showing a correlation peak at 0.65 m in surge and -0.38 m in sway.

tapered cosine function

$$P\left(y; y_1, y_2\right) = \begin{cases} 1, & |y| \leq y_1 \\ 0.5 + 0.5\cos\left(\pi \frac{y - y_1}{y_2 - y_1}\right), & y_1 < |y| \leq y_2 \\ 0, & |y| > y_2 \end{cases}, \tag{14}$$

where success is certain for sway magnitudes below y_1, failure is certain for sway magnitudes above y_2, and a gradual (raised cosine) transition occurs between these limits. The parameters y_1 and y_2 quantify the inter-pass sway tolerability. A similar approach could be taken to incorporate other factors (e.g., inter-pass yaw, seafloor complexity, etc.). However, validation and further development of these models is an area for future investigation.

IV. Experimental Results

Experimental data were used to demonstrate the concept proposed in Section II and to validate the model of Section III. These data were collected as part of the Multinational AutoNomy EXercise 2014 (MANEX '14), organised by the NATO Science and Technology Organisation (STO) Centre for Maritime Research and Experimentation (CMRE). The trial was carried out from the NATO Research Vessel (NRV) *Alliance* off the Italian coast near Levanto in September 2014. The data were collected using CMRE's Minehunting Unmanned underwater vehicle for Shallow water Covert Littoral Expeditions (MUSCLE).

MUSCLE is one of the primary systems employed in MCM sensing and autonomy research at CMRE [32]. It is a medium-sized Bluefin $21''$ (0.53 m) vehicle equipped with a Thales Underwater Systems SAS. The SAS operates at a carrier frequency of 300 kHz and a bandwidth of 60 kHz; the horizontal beamwidth of the real aperture is $5\,\mathrm{deg}$. The SAS image resolution is 2.5 cm $\times$ 1.5 cm (along-track $\times$ range) and the nominal range is 150 m with a 40 m nadir per side. The SAS processing software was developed by CMRE and implemented on the vehicle using graphics processing units (GPUs) for real-time processing. The navigation sub-system is comprised of a photonic inertial measurement unit, Teledyne

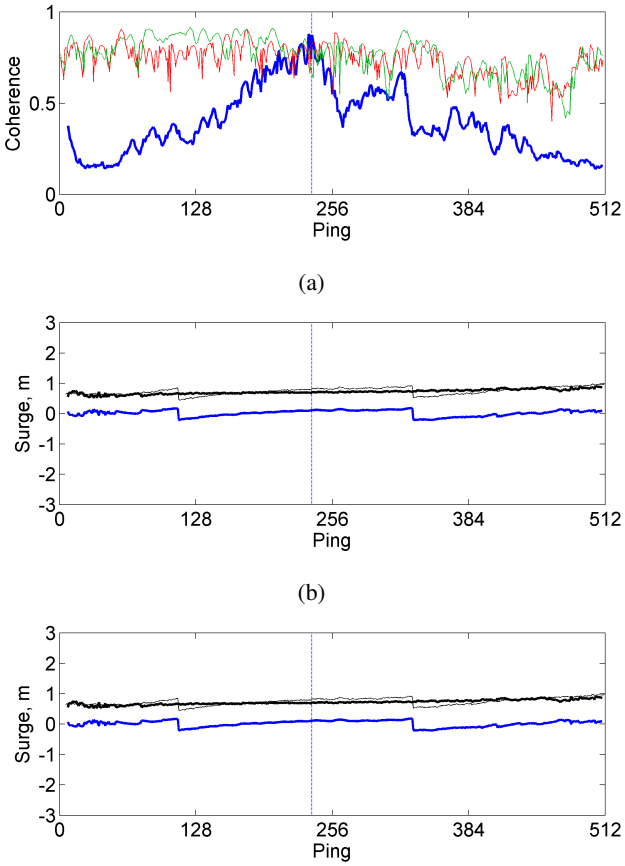

(a) (b) (c)

Fig. 5: RPC micronavigation at a slant-range of 85 m: (a) intra-pass coherence for the 11th track in red and 13th track in green, and the corresponding inter-pass coherence in blue; (b) inter-pass surge and (c) inter-pass sway for the same track pairs, where the thick blue lines show RPC estimates, the thin black lines show the navigation hardware measurements, and the thick black lines show the differences with means of 0.70 m in surge and -0.41 m in sway.

RDI-600 (600 kHz) Workhorse Navigator DVL [29], and a Novatel realtime kinematic (RTK) global positioning system (GPS) sensor.

In the experiment, a two-track pattern was repeated eleven times with a $1\,\mathrm{deg}$ heading increment between repetitions. Each track had a length of 330 m and was separated from the other by 150 m. The MUSCLE travelled at a speed of 1.5 m/s and an altitude of 10 m above the seafloor in a water depth of approximately 20 m. After executing each pattern, the vehicle surfaced for a GNSS fix and travelled along the sea surface to the start of the next one. A time of approximately 16 min, 30 s elapsed between each subsequent pattern. The tracks, as measured by DVL-aided INS, are shown in Figure 3.

A. Proof of Principle

The patterns that were executed in the experiment differ to those of both conventional paired-track patterns and the modified patterns proposed in Section II-B. Data-driven navigation estimation and correction was not performed by the vehicle in-situ. Furthermore, ground-truth measurements are not available to support the accuracy of any data-driven navigation estimates made in post-processing. Therefore, we do not claim to provide a proof of concept (this is a goal for future work). Instead, we present demonstrative proof of the basic principle. We do this by showing that a planned pattern of tracks can present many opportunities for repeated passes and that data-driven estimates of navigation drift can be made at each of these opportunities.

There are repeated passes along each combination of odd tracks (west-northwest heading) and each combination of even tracks (east-southeast heading) from the collection shown in Figure 3. However, we consider only the track combinations that are separated by nominal heading differences of $2\,\mathrm{deg}$ or less since this is the performance limit of repeat-pass RPC micronavigation for MUSCLE [24]. This yielded a total of 38 pairs of repeated passes. Data-driven navigation estimation was applied on each of these pairs using both incoherent image correlation and coherent repeat-pass RPC micronavigation. An example of the results from each approach is shown in Figure 4 and Figure 5, respectively.

SAS images were formed for each pass independently and registered to a common coordinate frame for each repeat-pass pair. Known geometric image transformations and distortions were accounted for based on the combined measurements from the navigation hardware and estimates from the intra-pass RPC micronavigation. Examples of two registered 50×50 m sub-images from the 11th and and 13th tracks (corresponding to the 6th and 7th pattern repetitions) are shown in Figure 4a and Figure 4b, respectively. The residual translations, which are attributed to navigation drift accumulated between passes, were measured by performing a 2-D cross-correlation and locating the peak. This was possible for all 38 pairs. The cross-correlation of the two example sub-images is shown in Figure 4c, where a peak is observed corresponding to an inter-pass surge error of 0.65 m and sway error of -0.38 m.

Inter-pass RPC micronavigation estimates were made using raw echo data from each pair of passes. 25 out of the 38 pairs (65%) had sufficient inter-pass coherence to perform the processing: 15/20 (75%) of those with 1 deg separation and 10/18 (55%) with 2 deg separation. Example results are shown from the same 11th and 13th tracks that were used above. The intra and inter-pass coherence values are plotted in Figure 5a and these are shown to attain a maximum value of approximately 0.9. High intra-pass coherence was maintained along the length of each pass but the inter-pass coherence varied due to decorrelation caused by footprint mismatch and baseline decorrelation effects [24]. The inter-pass surge and sway were estimated along portions of the repeated passes with sufficiently high inter-pass coherence. The differences between these estimates and the measurements from the navigation hardware were then computed. The repeat-pass RPC estimates, hardware measurements, and differences, which are attributed to navigation drift, are shown in Figure 5b and Figure 5c for surge and sway, respectively. The average value of inter-pass surge was 0.70 m and sway was -0.41 m.

Close agreement between the estimates obtained using incoherent and coherent estimation methods was observed for all of the considered pairs.

B. Model Validation

The navigation error model of Section III was validated using data from the experiment. The parameters of the MUSCLE navigation hardware were used as inputs to the model. However, to achieve agreement, it was necessary to apply a correction factor of 1.5 to the standard deviation values specified by the manufacturer (c.f., Table I). This is reasonable and accounts for various real-world influences, e.g., larger errors during diving and surfacing when the DVL bottom lock might be sub-optimal.

GNSS corrections were made by the navigation hardware after surfacing at the end of each pattern. These corrections provide measurements of the absolute navigation error that had accumulated after approximately 800 m of distance travelled. The magnitudes of the eleven GNSS measurements are plotted in Figure 6a. The corresponding histogram is shown in Figure 8a and the cumulative density function (CDF) is shown in Figure 8g. The modelled results are overlaid on the same plots for comparison. The modelled distribution of absolute error magnitudes is shown in Figure 6a as a function of the distance travelled and is represented by the mean, 50 percentile, and 90 percentile regions. The modelled histogram at the end of the pattern is shown in Figure 8d and the CDF is shown in Figure 8g. Good correspondence can be observed between the experimental results and the model. This has been supported quantitatively by a Kolmogorov-Smirnoff (KS) goodness-of-fit test [33] with a confidence of 95%. The KS test evaluates the statistical likelihood that samples were drawn from a reference probability distribution. In our application, the samples are the set of navigation errors measured by GNSS at the end of each pattern and the reference is our modeled error distribution.

The data-driven approaches provided relative estimates of the accumulated errors between the approximate centres of the odd and even track pairs, i.e., after approximately 165 m and 645 m of distance travelled, respectively. The magnitudes

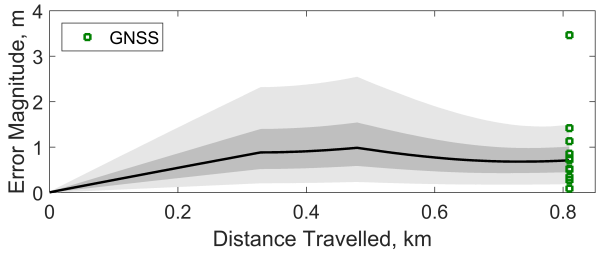

(a)

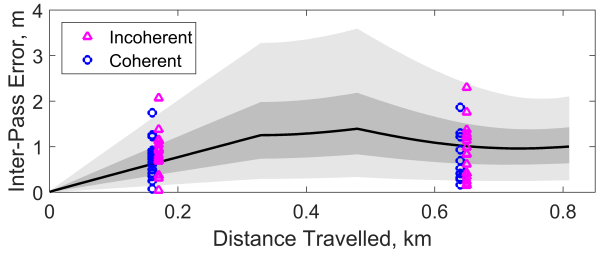

(b)

Fig. 6: Navigation errors for a pattern of two parallel 330 m tracks separated by 150 m (total distance traveled is 800 m): (a) error magnitudes and (b) relative error between repeated passes. The solid lines and shaded regions are the median, 50-percentile, and 90-percentile ranges from 10,000 Monte-Carlo simulations; in (a), the green markers are the measured errors from GNNS fixes; in (b), the triangular magenta markers are the inter-pass error estimates obtained by image correlation and the circular blue markers are the estimates obtained by repeat-pass micronavigation.

of the 38 incoherent estimates and 25 coherent estimates are plotted in Figure 6b together with the modelled profile of relative inter-pass errors. Further detail is provided in Figure 7, showing the along and across-track components of the error estimates from each method and the statistical distribution of the differences between methods. Comparison of the methods shows that image correlation tends to over-estimate both error components relative to repeat-pass micronavigation. Note that the rotation of the modelled error distribution in Figure 7b is caused by the correlated errors (primarily the DVL scale factor, in this case). The corresponding histograms for the inter-pass error magnitudes are shown in Figure 8b and Figure 8c for the experimental estimates and Figure 8e and Figure 8f for the model. The CDFs are shown in Figure 8h and Figure 8i. Again, good correspondence can be observed between the experimental and modelled distributions and this has been supported by KS tests with a confidence of 95%.

V. Performance Prediction

Clearly, the modified paired-track patterns will result in longer survey durations. However, this is the necessary trade-off for the improved navigation accuracy offered by the concept. In this section, we use the navigation error model to extrapolate for more realistic mission parameters. Thus, we make an initial attempt to quantify the trade-off. This has value

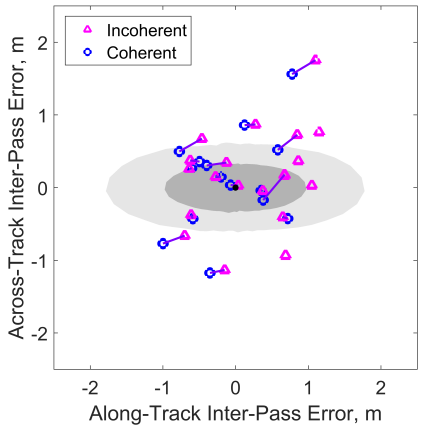

(a)

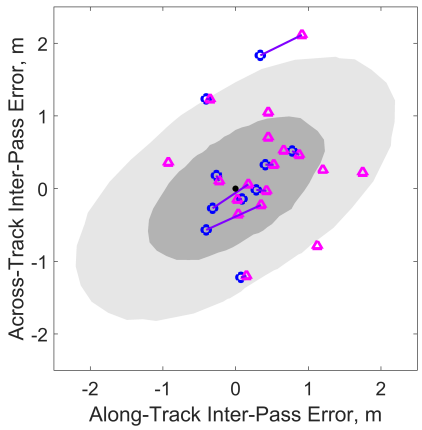

(b)

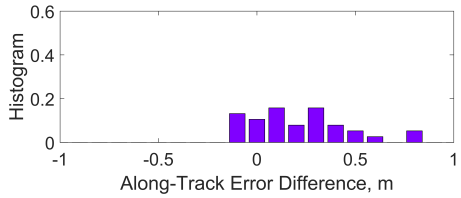

(c)

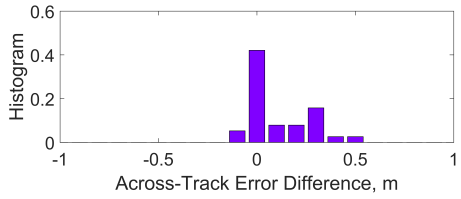

(d)

Fig. 7: Along and across-track components of the inter-pass navigation errors on the (a) first and (b) second tracks of the two-track pattern. The shaded regions are the median, 50-percentile, and 90-percentile ranges from 10,000 Monte-Carlo simulations; the triangular magenta markers are the estimates obtained by image correlation and the circular blue markers are the estimates obtained by repeat-pass micronavigation. The connecting lines between markers indicate corresponding estimates. The statistical distributions in (a) and (b) show the difference between estimates from the image correlation method relative to the micronavigation method.

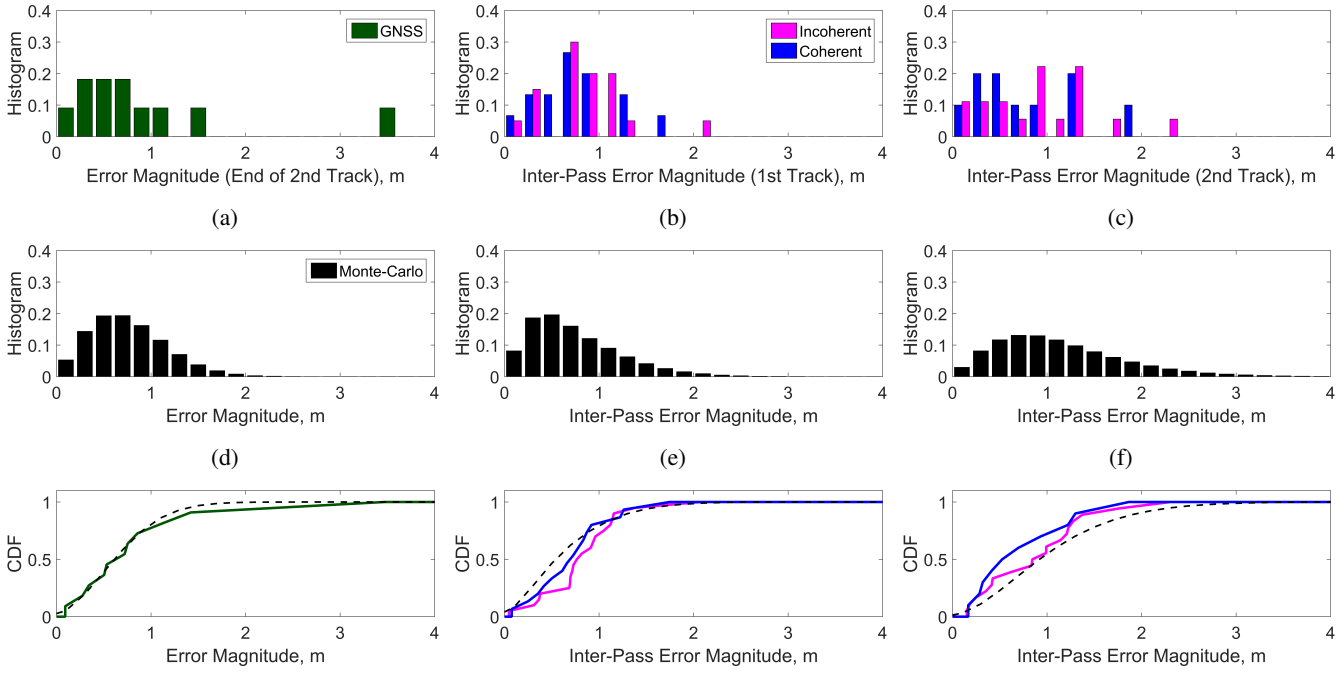

Fig. 8: Statistical distributions of navigation error magnitudes: (left column) at the end of the second track; (middle column) inter-pass error magnitudes in the center of the first track; and (right column) in the center of the second track. The top row shows experimental results from GNSS measurements in (a) and estimates obtained by data-driven methods in (b,c); the middle row (d,e,f) shows the corresponding modelled results from 10,000 Monte-Carlo simulations. Correspondence between the modelled and experimental results is demonstrated in the bottom row (g,h,i) by comparison of the cumulative density functions.

in informing and guiding future research and development of the concept.

We quantify the trade-off relative to a standard paired-track pattern using the percentage changes in the mission duration

$$\Delta T = (T - T_0)/T_0 \times 100\% \tag{15}$$

and the mean end-of-pattern navigation error

$$\Delta E = (E - E_0)/E_0 \times 100\%, \tag{16}$$

where T_0, E_0 are the duration and mean error for a conventional paired-track pattern and T, E are the duration and mean error for a modified pattern. Positive changes in duration are expected and negative changes in error are desired.

The survey times for each pattern can be calculated analytically. For a conventional paired-track pattern, the duration is given by

$$T_0 = \left[(2L + D_1)\,N + D_2\,(N-1)\right] \Big/ v \tag{17}$$

where L is the track length, D_1 is the intra-pair spacing, D_2 is the inter-pair spacing, N is the number of track pairs, and v is the vehicle speed. The modified paired track pattern uses two additional intra-pass tracks per pair, giving a duration of

$$T_1 = T_0 + 2D_1N/v, \tag{18}$$

and the split-modified paired track pattern uses four additional intra-pass tracks per pair, giving

$$T_2 = T_0 + 4D_1N/v. \tag{19}$$

The model parameters corresponding to the navigation hardware can be selected as described in Section IV-B. However, the parameters associated with the likelihood of successful drift estimation are not well understood. Moreover, these parameters depend on various factors, including the choice of estimation method, the properties of the sonar, and the operational and environmental conditions. The tolerability to inter-pass sway has been identified as a key factor influencing the drift estimation performance. For this reason, we consider it as a free variable and evaluate it over a range of possibilities.

MUSCLE is used as an illustrative example here. However, the same methodology can be applied to other systems. For MUSCLE, consistent seafloor coverage can be achieved using a paired-track pattern with an intra-pair spacing of approximately 80 m and an inter-pair spacing of approximately 160 m. This pattern and its modified variants are shown in Figure 2 for six track pairs of 1.5 km length. The model was used to predict the error distributions as a function of distance travelled for these patterns. A straight transit with a length equivalent to the conventional paired-track pattern (approximately 19 km) was also modelled for comparison.

The profile for the straight transit is shown in Figure 9a. It exhibits an increasing error over time, which results in a mean end-of-pattern error of approximately 40 m and a 50-percentile spread of ± 20 m. On the other hand, the profile of the paired-track pattern shown in Figure 9b exhibits a fluctuating error that increases less rapidly over time due to

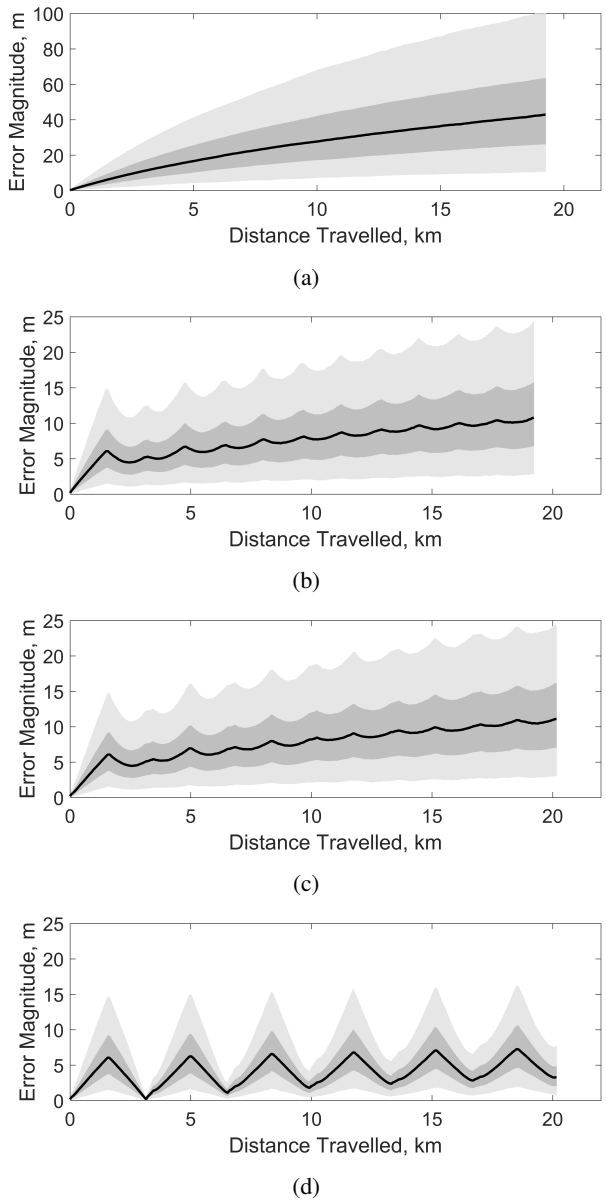

Fig. 9: Modelled navigation errors from 10,000 Monte-Carlo simulations for: (a) a straight transit of 19 km; (b) a conventional paired-track pattern with six pairs (total distance travelled is 19 km); (c) modified paired-track pattern (total distance travelled is 20 km); and (d) modified paired-track pattern assuming successful navigation correction at each repeated pass.

the partial cancellation of correlated error components along subsequent opposing tracks [30], [34]. Despite travelling the same distance, the mean end-of-pattern error in this case is approximately 10 m and the 50-percentile spread is approximately ±5 m. The profile of the modified pattern is shown in Figure 9c without navigation corrections and in Figure 9d with navigation corrections. In the latter case, it is assumed that all of the corrections were successful. Without corrections, the profile exhibits slightly higher end-of-pattern errors due to the longer travel distance of approximately 20 km. This is undesirable. However, with the corrections, the errors are reduced significantly in proximity to each repeated pass and the overall end-of-pattern error is reduced to approximately 5 m with 50-percentile spread of approximately ±2.5 m. The error profile in Figure 9d exhibits a "sawtooth" shape with troughs occurring where each data-driven navigation correction has been applied and peaks occurring at the furthest distances from each correction. In this idealised case, the trade-off is approximately a 5% increase in mission duration for a 50% decrease in navigation error.

A range of patterns with different sizes were modelled to investigate the scalability of the concept. Numbers of pairs from 1 to 15 were considered and track lengths were varied from 250 m to 4 km in steps of 250 m. The durations for each of the patterns were computed for a travel speed of 1.5 m/s. These are shown in Figure 10a for the conventional pattern and in 10b for the modified pattern. The percentage change between the two patterns is shown in 10c, where it can be observed that the change becomes less significant with longer tracks. The navigation errors were also modelled and a finite tolerability to inter-pass sway was considered by imposing a transition from probable success to probable failure at 10 m of inter-pass sway with a 10% transition region (i.e., $y_1 = 9.5$ m and $y_2 = 10.5$ m in (14)). Each pattern was modelled using 1,000 Monte-Carlo simulations. The modelled errors are shown in 10d and 10e for each of the patterns and the corresponding percentage change is shown in 10f. A decrease in the mean end-of-pattern error is observed in all cases. Furthermore, an optimal decrease in end-of-pattern error of approximately $50 - 75\%$ is reached for track lengths of approximately 1.5 km regardless of the number of track pairs; at this optimum, the corresponding increase in mission duration is approximately 5%.

The modelling was repeated with varying tolerability to inter-pass sway using transitions at 1 m, 2 m, 5 m, 10 m, 20 m, and 50 m with a 10% transition region. The resulting effects on navigation error are shown in Figure 11. Note that the change in survey duration remains unchanged. It can be observed that the reduction in navigation error becomes more significant as the tolerability to inter-pass sway increases. Furthermore, the optimal track length also increases with increasing tolerability.

Results for the alternative split-modified pattern are shown in Figure 12 for the survey duration and in Figure 13 for the end-of-pattern navigation error.

VI. Discussion of Results and Operational Impact

The value of the concept is driven by a trade-off between the utility of reducing navigation drift versus the cost of expending additional mission resources, i.e., energy and time. The modeling suggests that, under the right conditions, the accumulation of navigation errors can be reduced significantly without substantially increasing the survey duration. This can provide an operational advantage, particularly in applications where it is disadvantageous to surface regularly for a GNSS fix, e.g., during deep or covert missions.

The trade-off is influenced mostly by two factors: track length and tolerability of the estimation method to navigation drift.

The proportion of the survey that is dedicated to the redundant portions of the modified survey pattern decreases as the track length increases. Therefore, it is more efficient to choose longer tracks and fewer pairs when planning a mission. This is consistent with another important consideration of minimising the number of turns. On the other hand, longer tracks lead to greater accumulation of navigation errors between the repeated passes. While this introduces more potential for reducing the errors, if the accumulated drift is too high then the errors can exceed the tolerability of the estimation method (e.g., loss of coherence for repeat-pass RPC micronavigation or insufficiently matching features for image correlation) causing it to fail. In the extreme case, it can lead to a complete mismatch of the sensor footprints. This balance leads to the optima observed in Figure 10.

The results suggest that the trade-off can still be desirable below the optimum; they also appear to suggest the same beyond it (c.f., regions corresponding to long track lengths in Figure 10(c,d,e)). However, great care should be taken in making this interpretation of the statistics in the latter case. The plots show the mean outcome of many Monte-Carlo simulations and, beyond the optimum, the expected value for the change in error is negative (i.e., desirable) only because of a small imbalance between a very high reward (i.e., large reduction in navigation error) versus a high chance of failure. From an operational point of view, one cannot rely on the method to succeed in these cases.

The alternative split version of the pattern was proposed to mitigate the potential for failure due to the accumulation of too much drift during long tracks and / or for methods with low drift tolerance. For large search areas, this pattern can be repeated as necessary to cover the area, while maintaining the most effective track length for navigation corrections. In practice, selection of a modified pattern type (i.e., with or without a split or multiple splits) and associated estimation method will depend on the operational constraints, desired navigation accuracy, capabilities of the sonar system, and properties of the seafloor environment.

Some small inconsistencies were observed between the navigation error estimates from the two estimation methods, with the incoherent method tending to over-estimate both along and across-track error components relative to the incoherent method. This is likely to be caused by uncertainties in the assumed sound speed and bathymetry, which will affect both methods. These navigation correction errors have been assumed negligible in the performance prediction analysis. However, in future work they should be properly quantified alongside the probability of achieving a successful navigation correction.

Coherent estimation methods require a SAS-capable vehicle but provide higher precision than incoherent methods. Moreover, coherent methods can exploit acoustic speckle scattering regardless of a floor's geometric or radiometric structure, whereas incoherent methods rely on strong geometric and / or radiometric features. This motivates the use of coherent methods in benign seafloor environments and / or for short overlapping passes. However, on floors that are sufficiently feature-rich, incoherent methods are likely to be more tolerant to navigation errors than coherent methods. A pragmatic strategy for a SAS-capable vehicle is to use a coherent method when the repeat-pass coherence is sufficiently high and to revert to incoherent methods otherwise, possibly via an optimal fusion between methods.

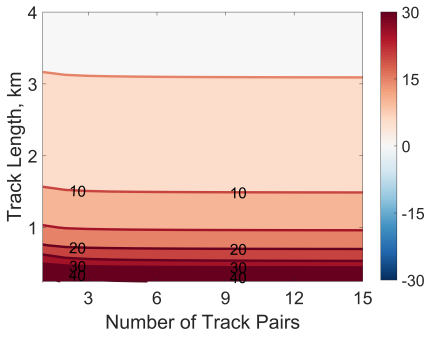

Fig. 12: Expected percentage change in the survey duration from a regular to the split-modified pattern.

In any case, the vehicle requires an on-board capability to process the data and to apply navigation corrections in-situ. Each correction should be back-propagated (e.g., by operating a Kalman filter backwards in time [7]) to fully exploit the information. However, this might be unnecessary in-situ unless it affects follow-on behaviors, such as revisiting targets or communicating their locations to collaborative vehicles.

VII. Conclusions

The preceding work has proposed a novel operational concept based on a variation of paired-track mission planning combined with data-driven navigation correction. The concept decreases both navigation drift and overall navigation error with a negligible increase on the mission duration or resources expended. When used in an underwater search mission, it can increase the accuracy of object localization, as well as ensuring that mission planning will provide sufficient high quality coverage to achieve the required mission performance. This concept was demonstrated using a Monte-Carlo model and validated using at-sea data from the MANEX '14 experiment.

The modification to the paired-track pattern requires a minimal increase in the overall mission length, equal to the product of the intra-pair track spacing and the number of track pairs. However, it provides opportunities to revisit previously covered areas of seafloor at the conclusion of each track pair, thus enabling the application of data-driven navigation correction. This allows for the accumulated drift to be corrected at the conclusion of each track pair.

We have demonstrated the application of two data-driven navigation correction methods – a coherent and an incoherent approach. While both provide reasonable corrections when an area on the seafloor is revisited, the coherent approach critically provides this ability on featureless seafloors, whereas incoherent methods rely on the presence of sufficient seafloor features. The coherent method provides the most flexibility

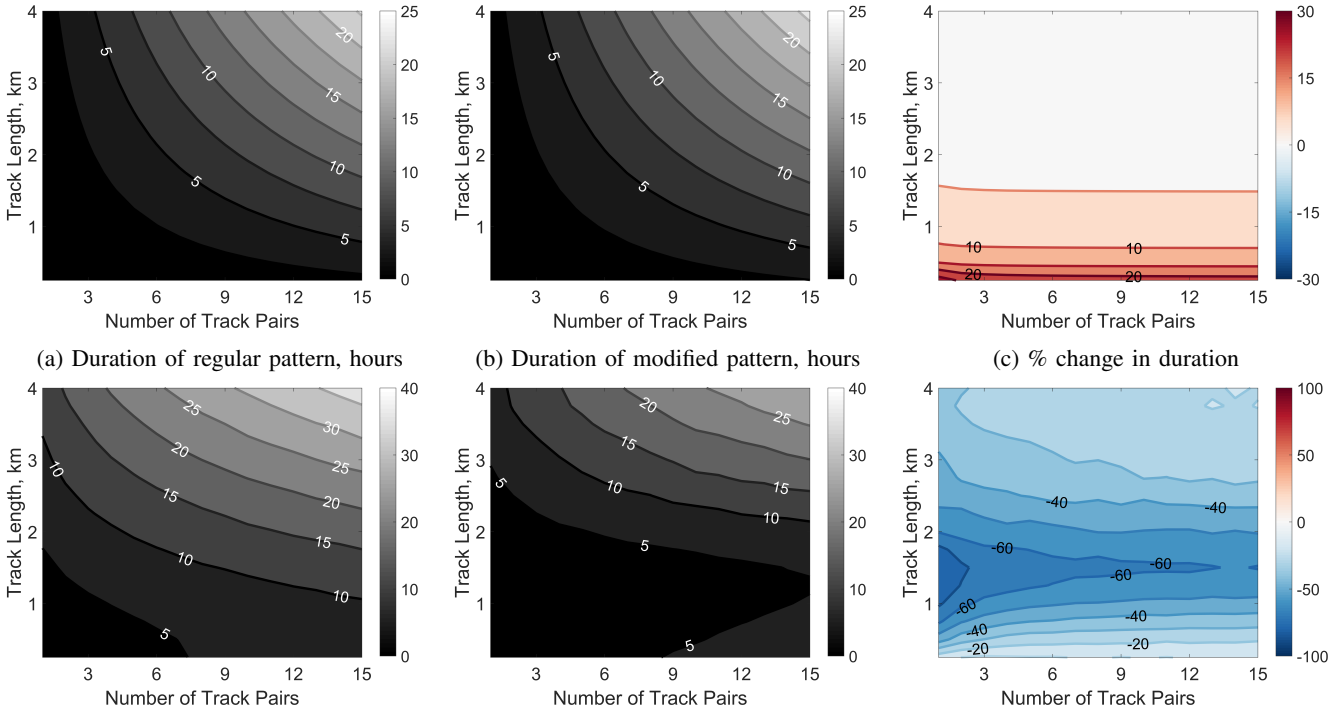

(a) Duration of regular pattern, hours (b) Duration of modified pattern, hours (c) % change in duration

(d) Error in regular pattern, m (e) Error in modified pattern, m (f) % change in error

Fig. 10: Expected survey times (top row) and end-of-survey navigation errors (bottom row) with respect to the survey parameters – number of paired tracks vs track length. A regular paired-track pattern is used in the left column and the modified paired-track pattern is used in the middle column, with a tolerability for repeat-pass sway of 10 m; the right column shows the percentage change from regular to the modified pattern.

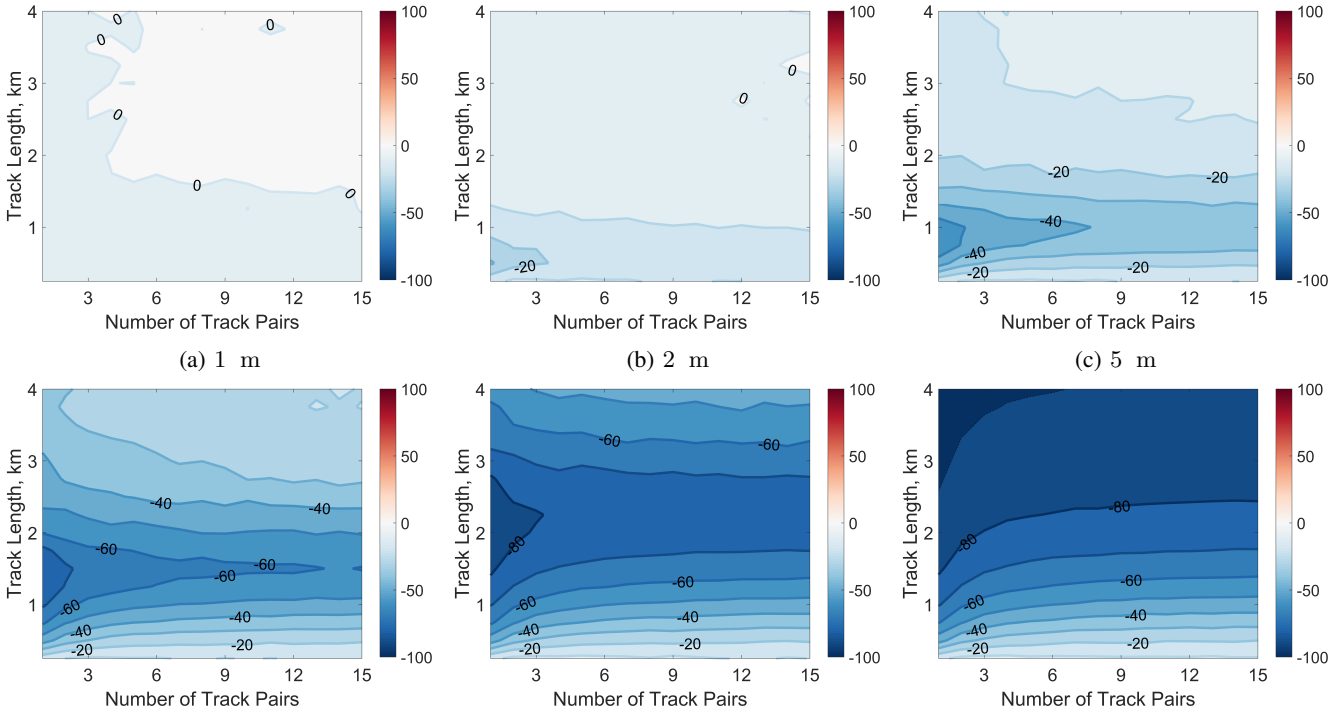

(a) 1 m (b) 2 m (c) 5 m

(d) 10 m (e) 20 m (f) 50 m

Fig. 11: Percentage change in navigation error with respect to tolerability in repeat-pass sway for the modified pattern.

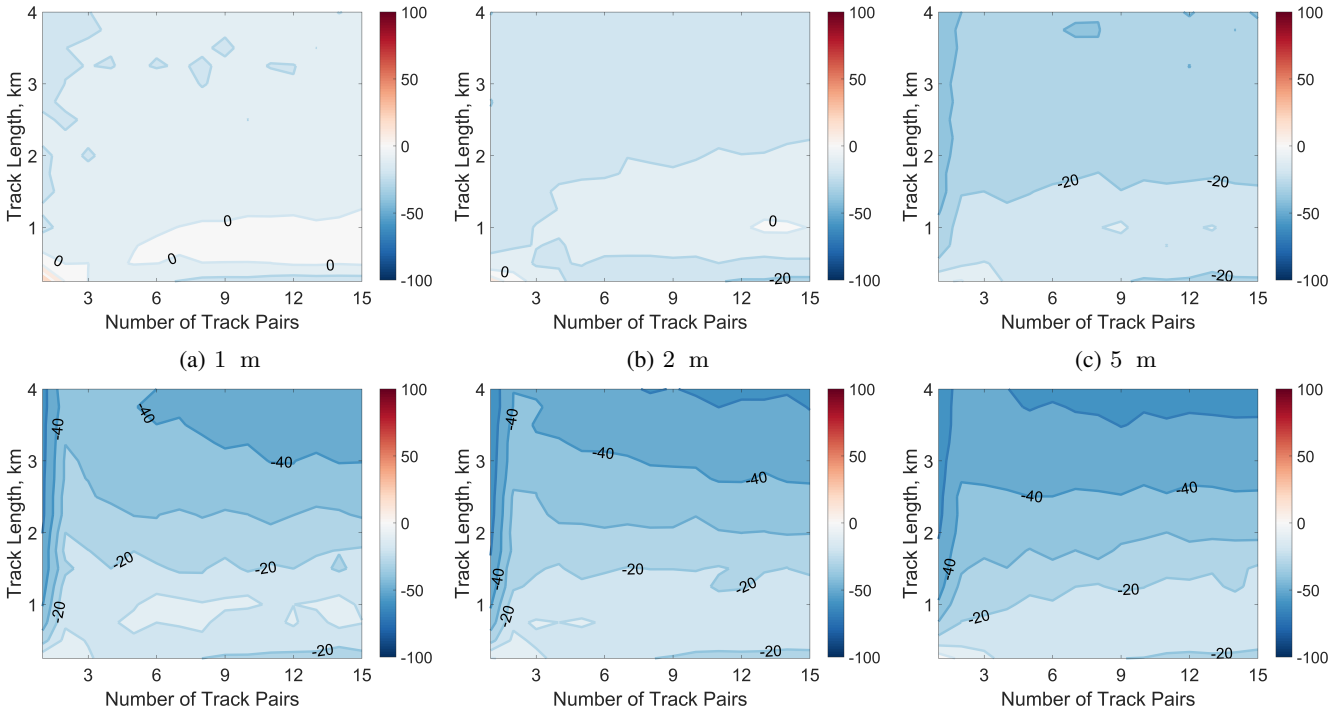

(a) 1 m (b) 2 m (c) 5 m

(d) 10 m (e) 20 m (f) 50 m

Fig. 13: Percentage change in navigation error with respect to tolerability in repeat-pass sway for the split-modified pattern.

in this sense, but its performance is more sensitive to the accumulation of sway errors. With the limitations of both methods considered, we have proposed an operational strategy to exploit the advantages of both methods when operating from a SAS-capable vehicle.

When considering an underwater search mission such as an MCM mission, accurate navigation and positioning is key to ensuring that detected objects can be reacquired and identified with a high probability and in a timely manner. Furthermore, effective mission planning requires an understanding of the expected navigation error to ensure that the prescribed quality of sensor coverage is achieved. Failure in either of these areas can result in wasted resources or the potential for coverage gaps. In time and resource-limited missions, neither are acceptable outcomes. Our concept provides a means of leveraging operational planning and sensor-based navigation to address these challenges posed by the unbounded accumulation of drift.

ACKNOWLEDGMENT

The authors would like to thank the crew of NRV Alliance during the MANEX '14 trial. Dr. Hunter is grateful to CMRE for hosting him during the summer of 2014.

REFERENCES

[1] A. Tal, I. Klein, and R. Katz, "Inertial navigation system/Doppler velocity log (INS/DVL) fusion with partial DVL measurements," *Sensors*, vol. 17, no. 2, Feb. 2017.

[2] B. Jalving, K. Gade, and E. Bovio, "Integrated inertial navigation systems for AUVs for REA applications," in *Proc. NURC MREP*, La Spezia, Italy, May 2003.

[3] J. C. Kinsey, R. M. Eustice, and L. L. Whitcomb, "A survey of underwater vehicle navigation: Recent advances and new challenges," in *Proceedings of the 7th IFAC Conference of Manoeuvring and Control of Marine Craft (MCMC)*, Lisbon, Portugal, 2006.

[4] I. Nygren and M. Jansson, "Terrain navigation for underwater vehicles using the correlator method," *IEEE J. Ocean. Eng.*, vol. 29, no. 3, pp. 906–915, July 2004.

[5] K. B. Ånonsen and O. K. Hagen, "Recent developments in the HUGIN AUV terrain navigation system," in *OCEANS 2011*, 2011.

[6] H. Durrant-Whyte and T. Bailey, "Simultaneous localisation and mapping (SLAM): Part I the essential algorithms," *IEEE Robot. Autom. Mag.*, vol. 13, no. 2, pp. 99–110, 2006.

[7] I. T. Ruiz, S. de Raucourt, Y. Petillot, and D. M. Lane, "Concurrent mapping and localization using sidescan sonar," *IEEE J. Ocean. Eng.*, vol. 29, no. 2, pp. 442–456, Apr. 2004.

[8] D. Ribas, P. Ridao, J. D. Tardós, and J. Neira, "Underwater SLAM in man-made structured environments," *Journal of Field Robotics*, vol. 25, no. 11–12, Nov–Dec 2008.

[9] E. Hernàndez, P. Ridao, D. Ribas, and J. Batlle, "MSISpIC: A probabilistic scan matching algorithm using a mechanical scanned imaging sonar," *Journal of Physical Agents*, vol. 3, no. 1, pp. 3–11, Jan. 2009.

[10] D. Forouher, J. Hartmann, M. Litza, and E. Maehle, "Sonar-based FastSLAM in an underwater environment using walls as features," in *15th International Conference on Advanced Robotics*, Tallinn, Estonia, June 2011.

[11] B. He, Y. Liang, X. Feng, R. Nian, T. Yan, M. Li, and S. Zhang, "AUV SLAM and experiments using a mechanical scanning forward-looking sonar," *Sensors*, vol. 12, no. 7, pp. 9386–9410, July 2012.

[12] M. F. Fallon, J. Folkesson, H. McClelland, and J. J. Leonard, "Relocating underwater features autonomously using sonar-based SLAM," *IEEE J. Ocean. Eng.*, vol. 38, no. 3, pp. 500–513, July 2013.

[13] C. Roman and H. Singh, "Improved vehicle based multibeam bathymetry using sub-maps and SLAM," in *IEEE/RSJ International Conference on Intelligent Robots and Systems*, Edmonton, Canada, Aug. 2005.

[14] P. Kimball and S. Rock, "Sonar-based iceberg-relative AUV navigation," *Deep Sea Research Part II: Topical Studies in Oceanography*, vol. 58, no. 11–12, pp. 1301–1310, June 2011.

[15] S. Barkby, S. B. Williams, O. Pizarro, and M. V. Jakuba, "A featureless approach to efficient bathymetric SLAM using distributed particle

mapping," *Journal of Field Robotics*, vol. 28, no. 1, pp. 19–39, Jan–Feb 2011.
[16] A. Palomer, P. Ridao, and D. Ribas, "Multibeam 3D underwater SLAM with probabilistic registration," *Sensors*, vol. 16, no. 4, Apr. 2016.
[17] J. Aulinas, X. Llado, and J. Salv, "Feature based SLAM using side-scan salient objects," in *IEEE/MTS Oceans*, Sydney, Australia, May 2010.
[18] K. Siantidis, "Side scan sonar based onboard SLAM system for autonomous underwater vehicles," in *IEEE/OES Autonomous Underwater Vehicles*, Tokyo, Japan, Nov. 2016.
[19] A. Bellettini and M. A. Pinto, "Theoretical accuracy of synthetic aperture sonar micronavigation using a displaced phase-center antenna," *IEEE J. Ocean. Eng.*, vol. 27, no. 4, pp. 780–789, Oct. 2002.
[20] M. P. Hayes and P. T. Gough, "Synthetic aperture sonar: a review of current status," *IEEE J. Ocean. Eng.*, vol. 34, no. 3, pp. 207–224, July 2009.
[21] J. Dillon, "Aided inertial navigation in GPS-denied environments using synthetic aperture processing," Defence Research and Development Canada, Halifax, Canada, Tech. Rep. DRDC-RDDC-2016-C200, Mar. 2016.
[22] S. A. V. Synnes, H. J. Callow, R. E. Hansen, and T. O. Sæbø, "Multipass coherent processing on synthetic aperture sonar data," in *Proc. European Conference on Underwater Acoustics (ECUA)*, Istanbul, Turkey, July 2010.
[23] A. J. Hunter, S. Dugelay, and W. J. Fox, "Repeat-pass synthetic aperture sonar micronavigation using redundant phase center arrays," *IEEE J. Ocean. Eng.*, vol. 41, no. 4, Oct. 2016.
[24] A. J. Hunter and S. Dugelay, "Exploiting the coherence of seabed scattering for repeat-pass SAS," in *Proc. International Conference on Seabed and Sediment Acoustics: Measurements and Modelling*. Bath, UK: Institute of Acoustics, Sept. 2015.
[25] A. P. Lyons and D. C. Brown, "The impact of the temporal variability of sea floor roughness on synthetic aperture sonar repeatpass interferometry," *IEEE J. Ocean. Eng.*, vol. 38, no. 1, pp. 91–97, Jan. 2013.
[26] T. G-Michael, T. M. Marston, and D. D. Sternlicht, "Image-based automated change detection for synthetic aperture sonar by multistage coregistration and canonical correlation analysis," *IEEE J. Ocean. Eng.*, vol. 41, no. 3, pp. 592–612, July 2016.
[27] V. T. Wang and M. P. Hayes, "Synthetic aperture sonar track registration usingn SIFT image correspondences," *IEEE J. Ocean. Eng.*, 2017.
[28] K. Gade, "NAVLAB, a generic simulation and post-processing tool for navigation," *European Journal of Navigation*, vol. 2, no. 4, pp. 135–150, Nov. 2004.
[29] Teledyne RD Instruments, *Workhorse Navigator Doppler Velocity Log (DVL) Datasheet*, nav-1004 Rev. July 2013.
[30] B. Jalving, K. Gade, K. Svartveit, A. Willumsen, and R. Sførhagen, "DVL velocity aiding in the HUGIN 1000 integrated inertial navigation system," in *ADCPs in Action*, Nice, France, June 2004.
[31] L. Bartosch, "Generation of colored noise," *International Journal of Modern Physics C*, vol. 12, no. 6, pp. 851–855, 2001.
[32] A. Bellettini and M. A. Pinto, "Design and experimental results of a 300-khz synthetic aperture sonar optimized for shallow-water operations," *IEEE J. Ocean. Eng.*, vol. 34, no. 3, pp. 285–293, July 2009.
[33] F. J. Massey, "The Kolmogorov-Smirnov test for goodness of fit," *J. Amer. Statist. Assoc.*, vol. 46, no. 253, pp. 68–78, Mar. 1951.
[34] A. J. Hunter and W. A. Connors, "Statistics of an autoregressive correlated random walk along a return path," *IET Electron. Lett.*, Sep 2017.

Alan J. Hunter was born in Christchurch, New Zealand, in 1978. He received the B.E.(Hons) and Ph.D. degrees in electrical and electronic engineering from the University of Canterbury (NZ) in 2001 and 2006, respectively. From 2007 to 2010, he was a research associate at the University of Bristol, England and from 2010 to 2014 he was a defense scientist at TNO (Netherlands Organisation for Applied Scientific Research), The Netherlands. Since 2014, Dr. Hunter has been a lecturer in the Faculty of Engineering and Design at the University of Bath, England. Since 2017, he has also been an adjust associate professor in the Department of Informatics at the University of Oslo, Norway. Dr. Hunter's research interests are in underwater acoustics, sonar imaging of the seafloor, and autonomous underwater systems.

Warren A. Connors was born in Saint John New Brunswick, Canada in 1976. He received a B.Sc. and M.Sc in Computer Science (Machine Learning) from Dalhousie University in 2001 and 2013 respectively. In 2000 he joined MDA where he was primarily involved in software systems engineering for mine countermeasures. In 2007 he joined the mine countermeasures group Defence Research and Development Canada, working in autonomy and perception for robotic MCM systems. Since 2014, Warren has been working at the NATO Centre for Maritime Research and Experimentation in La Spezia, Italy, working in autonomy as well as planning and evaluation techniques for autonomous MCM. Warren's research interests are in autonomy for communications limited environments, machine learning, cognitive robotics, defence applications of robotics and autonomous underwater systems.

Samantha Dugelay was born in London, England in 1969. She received a B.Sc. and M.Sc. in Mathematics from the Université de Bretagne Occidentale, Brest, France in 1991 and 1993 respectively, a Diplôme d'Études Approfondies in Statistical and Stochastic Modelling in 1994 and a Ph.D. degree in Mathematics in 1997 both from the Université de Paris Sud, Orsay, France. From 1997 to 2000 she worked as a research associate at University College London and then the University of Bath, England. She joined QinetiQ in 2000 as a Senior Scientist and then transferred to Dstl in 2006 as a technical lead for MCM sensor requirements and MCM automatic target recognition. Since 2013, Samantha has been working at the Centre for Maritime Research and Experimentation in La Spezia, Italy as the project leader on Autonomous Mine Search. Dr Dugelay's interests lie in autonomous maritime vehicles, underwater acoustics and sonar data processing.